Influence of alkyl spacer in nanostructure shape control by templateless electropolymerization

Salif Sow, Fatoumata Sow, Abdoulaye Dramé, François Orange, Aboubacary Sene, Samba Yandé Dieng, Frédéric Guittard, Thierry Darmanin

Influence of alkyl spacer in nanostructure shape control by templateless electropolymerization

Salif Sow[a], Fatoumata Sow[a], Abdoulaye Dramé[a], François Orange[b], Aboubacary Sene[a], Samba Yandé Dieng[a], Frédéric Guittard[c,d] and Thierry Darmanin[c,*]

[a]*Université Cheikh Anta Diop, Faculté des Sciences et Techniques, Département de Chimie, B.P. 5005 Dakar, Sénégal.*

[b]*Université Côte d'Azur, CCMA, 06100, Nice, France.*

[c]*Université Côte d'Azur, NICE Lab, Parc Valrose, 06200 Nice, France.*

Corresponding author: thierry.darmanin@unice.fr

[d]*University California Riverside, Department of Bioengineering, Riverside, CA, USA*

Abstract

Here, we control the shape of the resulting porous structures by templateless electropolymerization, by adjusting the alkyl spacer between thieno[3,4-*b*]thiophene and pyrene used as the monomer and the substituent, respectively. A huge change is observed from nanotubular structures (1D growth) without alkyl chain to huge hollow spheres (3D growth) for longer alkyl chains ($\geq C_4H_8$) passing through ribbon-like structures (2D) for short C_2H_4 spacer. The presence of a significant amount of water is necessary for the formation of these porous structures because it allows releasing a high amount of gas bubbles. Moreover, this change in surface structures is also observed by varying H_2O content. Here, the higher hydrophobic properties with extremely high water adhesion are obtained with the presence of ribbon-like structures. This work is extremely important to investigate the effect of surface structures on surface properties for various potential applications.

Keywords: Nanotubes, Nanostructures, Electrochemistry, Conducting polymers, Wettability.

Introduction

The difficulty in obtaining regular nanoscale order at low cost is a key challenge when engineering materials for applications in sensors, photocatalysis, energy storage, photovoltaics, drug delivery, and biomedical imaging [1–5]. The dimensions of these features (diameter, height, porosity, shape) significantly impact on macroscopic surface properties, most notably wettability [6–11]. A unique aspect of nanotubular and nanoporous structures, which makes them particularly interesting to study, is that the air trapped within nanotubes significantly impacts the macroscopic surface hydrophobicity and water adhesion [12–14]. Beyond their overall impact on surface properties and applications in interfacial engineering, vertically aligned structures are also omnipresent in nature (gecko toepads, plant and leaf surfaces) and biology (tissue architectures) [15–18]. Therefore, identifying methods to replicate these naturally formed structures provides unique avenues to study natural systems and also to implement bioinspiration when addressing engineering challenges.

The preparation of well-ordered nanoporous structures such as vertically aligned nanotubes have typically been made using hard templates, such as anodized aluminum oxide (AAO) membranes which specifically direct the formation of surface features [19–24]. This strategy is quite labor-intensive and the membranes are often "single-use". Even if the membranes can be used repeatedly a totally new membrane is required to manipulate a single nanotube parameter (e.g. height, diameter, etc.).

By contrast, templateless electropolymerization is an excellent alternative. Gas bubbles produced *in-situ* during electropolymerization can act as a soft template, thus eliminating any hard or pre-formed template to direct growth of tubular features. In the literature, templateless electropolymerization of pyrrole in water (H_2O) has been specifically studied [25–33]. The formation of porous structures is induced by the release of gas bubbles (H_2 and/or O_2) while a surfactant is necessary to stabilize them and induce the polymer growth around them. For example, two strategies were reported either by potentiostatic methods (such as constant potential) in order to release O_2 bubbles [25–28] or potentiodynamic methods (such as cyclic voltammetry) but in the presence of an acid in order to release H_2 bubbles [29–32]. It is worth noting that Margaritondo and co-workers observed by real-time microradiography during electropolymerization of pyrrole in water that the microcontainer shape can be obtained by deformation force around H_2 bubbles at the three-phase boundary changing the shape from spherical to elliptical and then to cylindrical [32].

Very recently, the process was performed also in organic solvent such as dichloromethane (CH_2Cl_2). It is a notable advance because most of the monomers are not soluble in water and electropolymerization in appropriate organic solvents can be performed at low monomer

concentration. By chemical tuning of the used monomer, it is possible to obtain various nanotubular structures without surfactant nor acid and even at low H_2O content (H_2O naturally present in solution). Different porous structures including very well-ordered vertically aligned nanotubes with high water adhesion are reported using 3,4-phenylenedioxythiophene (PheDOT), 3,4-naphthalenedioxythiophene (NaphDOT) and thieno[3,4-*b*]thiophene derivatives [34–41].

Using thieno[3,4-*b*]thiophene-based monomers, it was reported unique results with pyrene as the substituent because it participates to electropolymerization and also induces high π-sticking interaction [35–38]. Here, we have wanted to study how an alkyl spacer between the monomer core and the substituent (Scheme 1) can modify the polymer growth around gas bubbles leading to different surface structures. Moreover, the surface structures being highly affected by water content as clearly demonstrated in the literature [40], two different solvents are investigated: CH_2Cl_2 and CH_2Cl_2 saturated with H_2O (named here CH_2Cl_2 + H_2O sat.).

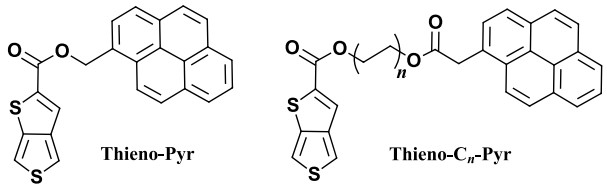

Scheme 1. Investigated monomers in this manuscript (n = 2, 4, 6, 8 and 10).

2. Experimental Section

2.1. Monomer synthesis

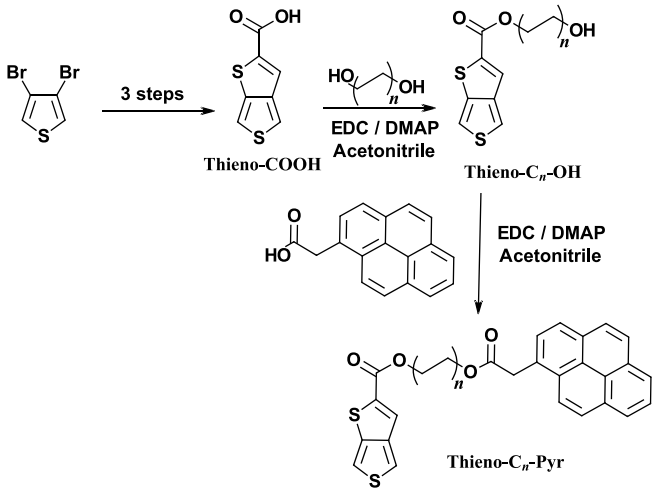

Scheme 2. Chemical way to the monomers.

Pyren-1-ylmethyl thieno[3,4-*b*]thiophene-2-carboxylate (Thieno-Pyr) was synthesized using a previously reported procedure [43–45]. For the original monomers, thieno[3,4-*b*]thiophene-2-carboxylic acid (Thieno-COOH) was synthesized in three steps from 3,4-dibromothiophene. After, 1.0 eq (200 mg) of Thieno-COOH was dissolved in 20 mL of anhydrous acetonitrile in a 100 mL flask in the presence of 1.2 eq of EDC and 20 mg of DMAP (1.6 %). After 30 min, 1.5 eq of a selected linear diol was added previously dissolved in acetonitrile. The mixture was stirred at room temperature for 24 h. The products were purified by column chromatography on silica gel (ether / cyclohexane same volume as eluant) to obtain the alcohols (NMR spectra are available in ESI).

Thieno-C$_2$-OH: 2-hydroxyethyl thieno[3,4-*b*]thiophene-2-carboxylate. Yield 58%; Yellow oil; δ_H(400 MHz, $CDCl_3$): 7.74 (s, 1H), 7.61 (d, 1H, J = 2.4 Hz), 7.30 (dd, J = 2.7 Hz, J = 0.8 Hz, 1H), 4.47 (t, J = 4.4 Hz, 2H), 3.95 (m, 2H), 2.05 (s, 1H); δ_C(400 MHz, $CDCl_3$): 163.36, 145.77, 139.72, 138.92, 124.08, 116.96, 111.47, 65.14, 61.21; MS (70 eV): m/z 228 (M^+, 50), 184 ($C_7H_4O_2S_2^+$, 100), 167 ($C_7H_3OS_2^+$, 70).

Thieno-C$_4$-OH: 4-hydroxybutyl thieno[3,4-*b*]thiophene-2-carboxylate. Yield 21%; Orange oil; δ_H(400 MHz, $CDCl_3$): 7.71 (s, 1H), 7.60 (d, J = 2.4 Hz, 1H), 7.29 (dd, J = 2.7 Hz, J = 1.0 Hz, 1H), 4.36 (t, 2H, J = 6.4 Hz), 3.74 (t, J = 6.4 Hz, 2H), 3.08 (s, 1H), 1.87 (m, 2H), 1.73 (m, 2H); δ_C(400 MHz, $CDCl_3$): 163.16, 145.91, 139.15, 123.59, 116.72, 111.41, 65.40, 62.38, 29,17, 25.18 ; MS (70 eV): m/z 256 (M+, 25), 184 ($C_7H_4OS_2^+$, 100), 167 ($C_7H_3OS_2^+$, 30).

Thieno-C$_6$-OH: 6-hydroxyhexyl thieno[3,4-*b*]thiophene-2-carboxylate. Yield 26%; Orangeoil; δ_H(400 MHz, $CDCl_3$): 7.63 (s, 1H), 7.53 (d, J = 2.4 Hz, 1H), 7.22 (dd, J = 2.7 Hz, J = 0.8 Hz, 1H), 4.25 (t, J = 6.4 Hz, 2H), 3.60 (t, J = 6.4 Hz, 2H), 1.79 (m, 2H), 1.61 (m, 2H), 1.47 (s, 1H), 1.43 (m, 5H); δ_C(400 MHz, CDCl3): 163.20, 145.93, 139.78, 123.47, 116.61,

111.35, 65.53, 62.81, 32.58, 28,59, 25.73, 25.36; MS (70 eV): m/z 284 (M+, 25), 184 ($C_7H_4O_2S_2^+$, 100), 167 ($C_7H_3OS_2^+$, 30).

Thieno-C_8-OH: 8-hydroxyoctyl thieno[3,4-*b*]thiophene-2-carboxylate. Yield 20%; Orange oil; δ_H(400 MHz, $CDCl_3$): 7.70 (s, 1H), 7.60 (d, J = 2.6 Hz, 1H), 7.28 (dd, J = 2.7 Hz, J = 0.8 Hz, 1H), 4.32 (t, J = 6.6 Hz, 2H), 3.63 (t, J = 6.4 Hz, 2H), 1.75 (m, 2H), 1.60 (m, 2H), 1.45 (m, 8H); δ_C(400 MHz, $CDCl_3$): 163.21, 145.94, 139.81, 123.45, 116.61, 111.36, 65.70, 63.02, 32.74, 29,28, 29.18, 28.62, 25.87, 25.65; MS (70 eV): m/z 312 (M+, 10), 184 ($C_7H_4OS_2^+$, 100), 168 ($C_7H_4OS_2^+$, 95).

Thieno-C_{10}-OH: 10-hydroxydecyl thieno[3,4-b]thiophene-2-carboxylate. Yield 25%; Orange oil; δ_H(400 MHz, $CDCl_3$): 7.70 (s, 1H), 7.60 (d, J = 3.2 Hz, 1H), 7.29 (dd, J = 2.7 Hz, J = 0.8 Hz, 1H), 4.30 (t, J = 6.6 Hz, 2H), 3.64 (t, J = 6.4 Hz, 2H), 1.75 (m, 2H), 1.56 (m, 2H), 1.40 (m, 12H); δ_C(400 MHz, $CDCl_3$): 163.21, 145.94, 139.84, 123.42, 116.58, 111.36, 65.70, 63.08, 32.74, 29,28, 29.18, 28.62, 25.92, 25.91, 25.87, 25.72; MS (70 eV): m/z 340 (M+, 10), 184 ($C_7H_4O_2S_2^+$, 60), 168 ($C_7H_4OS_2^+$, 100).

The monomers were synthesized by reacting 1-Pyreneacetic acid with Thieno-C_n-OH via a simple esterification reaction (Scheme 2). Briefly 1.2 eq of 1-Pyreneacetic acid was dissolved in 20 mL of acetonitrile in the presence of 1.2 eq of EDC and 20 mg of DMAP or (1.6 mmol) with stirring at room temperature for 30 minutes. Then, Thieno-C_n-OH dissolved in acetonitrile was added. After 24 hours, the products were purified by chromatography on a column of silica gel (ether / cyclohexane, same volume as eluent).

Thieno-C_2-Pyr: 2-(2-(5,9-dihydropyren-1-yl)acetoxy)ethyl thieno[3,4-b]thiophene-2-carboxylate. Yield 58%; Orange oil; δ_H(400 MHz, $CDCl_3$): 8.25 (d, J = 9.2 Hz, 1H), 8.09 (m, 4H), 7.95 (m, 4H), 7.28 (d, J = 2.7 Hz, 1H), 7.22 (s, 1H), 7.12 (dd, J = 2.7 Hz, J = 0.7 Hz, 1H), 4.49 (m, 4H), 4.41 (s, 2H); δ_C(400 MHz, $CDCl_3$): 171.28, 162.62, 145.57, 139.60, 138.52, 131.15, 130.79, 130.65, 129.37, 128.38, 127.94, 127.24, 125.85, 125.18, 125.05, 124.94, 124.81, 124.58, 123.68, 123.09, 116.73, 111.10, 62.92, 62.21, 39.43.

Thieno-C_4-Pyr: 4-(2-(3,9-dihydropyren-1-yl)acetoxy)butyl thieno[3,4-*b*]thiophene-2-carboxylate. Yield 38%; Orange oil; δ_H(400 MHz, $CDCl_3$): 8.28 (d, J = 9.3 Hz, 1H), 8.15 (m, 4H), 8.05 (m, 4H), 7.68 (s, 1H), 7.57 (d, J = 2.7 Hz, 1H), 7.27 (dd, J = 2.7 Hz, J = 0.7 Hz, 1H), 4.36 (s, 2H), 4.21 (m, 4H), 1.72 (m, 4H); δ_C(400 MHz, $CDCl_3$): 171.55, 162.94, 145.84, 139.42, 138.86, 131.27, 130.79, 130.69, 129.37, 128.09, 127.91, 127.32, 125.96, 125.25, 125.10, 125.00, 124.86, 124.69, 123.51, 123.00, 116.67, 111.34, 64.90, 64.45, 39.75, 39.60, 26.90, 25.23.

Thieno-C_6-Pyr: 6-(2-(5,9-dihydropyren-1-yl)acetoxy)hexyl thieno0[3,4-*b*]thiophene-2-carboxylate. Yield 35%; Orange oil; δ_H(400 MHz, $CDCl_3$): 8.27 (d, J = 9.3 Hz, 1H), 8.15 (m, 4H), 8.05 (m, 4H), 7.65 (s, 1H), 7.57 (d, J = 2.7 Hz, 1H), 7.27 (dd, J = 2.7 Hz, J = 0.7 Hz, 1H), 4.34 (s, 2H), 4.11 (m, 4H), 1.60 (m, 4H), 1.26 (m, 4H); δ_C(400 MHz, $CDCl_3$): 170.47, 166.84, 158.48, 155.00, 148.46, 147.00, 146.69, 142.18, 140.99, 139.80, 139.20, 133.47, 133.15, 130.78, 128.37, 127.84, 127.41, 126.00, 124.88, 123.44, 116.63, 111.84, 65.35, 64.89, 28.42, 28.37, 26.93, 25.44, 24.67.

Thieno-C_8-Pyr: 8-(2-(5,9-dihydropyren-1-yl)acetoxy)octyl thieno[3,4-*b*]thiophene-2-carboxylate. Yield 38%; Orange oil; δ_H(400 MHz, $CDCl_3$): 8.28 (d, J = 9.3 Hz, 1H), 8.15 (m, 4H), 8.05 (m, 4H), 7.68 (s, 1H), 7.57 (d, J = 2.7 Hz, 1H), 7.27 (dd, J = 2.7 Hz, J = 0.7 Hz, 1H), 4.34 (s, 2H), 4.22 (t, J = 6.5 Hz, 2H), 4.09 (t, J = 6.5 Hz, 2H), 1.57 (m, 6H), 1.22 (m, 6H); δ_C(400 MHz, $CDCl_3$): 171.66, 163.14, 157.24, 155.00, 148.46, 147.90, 146.46, 142.18, 140.52, 139.79, 139.20, 133.47, 133.15, 130.78, 128.38, 128.31, 127.84, 127.25, 125.97, 124.77, 123.33, 116.57, 111.34, 65.60, 65.05, 39.74, 28.94, 28.88, 28.46, 26.90, 25.66.

Thieno-C_{10}-Pyr: 10-(2-(5,9-dihydropyren-1-yl)acetoxy)decyl thieno[3,4-*b*]thiophene-2-carboxylate. Yield 42%; Orange oil; δ_H(400 MHz, $CDCl_3$): 8.28 (d, J = 9.3 Hz, 1H), 8.15 (m, 4H), 8.05 (m, 4H), 7.69 (s, 1H), 7.57 (d, J = 2.7 Hz, 1H), 7.27 (dd, J = 2.7 Hz, J = 0.7 Hz, 1H), 4.43 (s, 2H), 4.34 (t, J = 6.6 Hz, 2H), 4.11 (t, J = 6.6 Hz, 2H), 1.74 (m, 2H), 1.56 (m, 4H), 1.28 (m, 10H); δ_C(400 MHz, $CDCl_3$): 171.69, 163.22, 159.01, 156.32, 148.94, 145.67, 139.81, 139.21, 137.84, 137.79, 133.88, 132.60, 131.32, 130.78, 128.38, 128.36, 127.88, 127.27, 125.98, 124.86, 123.36, 116.57, 111.35, 65.73, 65.15, 39.79, 29.26, 29.11, 29.04, 28.61, 28.52, 26.93, 25.85, 25.75.

2.2. Electropolymerization parameters

The templateless electropolymerization was performed using a potentiostat (Autolab from Metrohm). 2 cm^2 gold-coated silicon wafers were used as working electrode. The electrolyte used was tetrabutylammonium perchlorate (Bu_4NClO_4). The solvents were tested either dichloromethane (CH_2Cl_2) or CH_2Cl_2 saturated with H_2O (called here CH_2Cl_2 + H_2O sat.). Here, it was chosen to saturate CH_2Cl_2 with H_2O because of the low solubility of H_2O in CH_2Cl_2 (around 0.15 g/100 mL). CH_2Cl_2 + H_2O sat. was simply prepared by mixing CH_2Cl_2 with a high amount of H_2O and removing any excess H_2O by extraction after decantation. Then, the depositions were performed by cyclic voltammetry from -1 V to monomer

oxidation potential (E^{ox} ≈ 1.55–1.65 V *vs* SCE depending on the monomers) at a scan rate of 20 mV s^{-1}. Different numbers of scans (1, 3 and 5) were tested in order to study the polymer growth. After deposition, the substrates were washed three times in CH_2Cl_2 and slowly dried.

2.3. Surface characterization

After metallization, surfaces structures were imaged *via* scanning electron microscopy (SEM) (6700F microscope from JEOL). The surface wettability was characterized *via* goniometer (DSA30 from Bruker) with 2 μL water droplets and by measuring the apparent contact angles with water (θ_w) taken at the triple point (n=5). The arithmetic (Ra) and quadratic (Rq) surface roughness were determined *via* optical profiling system (WYKO NT1100 from Bruker). The measurements were realized with the working mode High Mag Phase Shift Interference (PSI), the objective 20X, and the field of view 0.5X. The surface chemistry was characterized by EDX analyses with a Tescan Vega 3 XMU scanning electron microscope (TESCAN FRANCE, Fuveau, France) equipped with an X-MaxN 50 EDX detector (Oxford Instruments, Abingdon, U.K.). Prior to analyses, the samples were carbon-coated and the analyses performed under identical conditions: an acceleration voltage of 10 kV, a 10 mm working distance and a 2000× magnification. EDX spectra were processed with the Aztec software (version 3.1, Oxford Instruments).

3. Results and Discussion

Here, two solvents were chosen in order to release different amounts of gas. First, dichloromethane (CH_2Cl_2) was selected because previous works show that porous structures can be formed depending on the monomer even if the water content is very low. Then, a dichloromethane solution saturated with H_2O (named here CH_2Cl_2 + H_2O sat.) was also tested in order to release a much high amount of gas (O_2 and/or H_2 depending on electrodeposition method). Indeed, comparing the cyclic voltammogram of the two solvents, a large peak at ≈ -0.5 V *vs* SCE is clearly apparent during the back scan, but only for CH_2Cl_2 + H_2O sat. and not in CH_2Cl_2 confirming the reaction $2\ H_2O + 2\ e^- \rightarrow \mathbf{H_2}$ (bubbles) + $2\ OH^-$. The peak starts at ≈ -0.0 V and extends to ≈ -0.85 V. Another peak is also present during the forward scan, indicative of the reaction $2\ H_2O \rightarrow \mathbf{O_2}$ (bubbles) + $4\ H^+ + 4\ e^-$ but this one starts only at ≈ 2.0 V *vs* SCE. Then, the monomers were added and their oxidation potential (E^{ox}) was found to

be ≈ 1.55–1.65 V *vs* SCE. It is expected here than the oxidation potential of thienothiophene is lower than that of thiophene due to conjugation between the two thiophene rings, for example. Hence, cyclic voltammetry (from -1 V to E^{ox}) was chosen as the electropolymerization method and H_2 gas bubbles are mainly expected during the back scans in the used potential range.

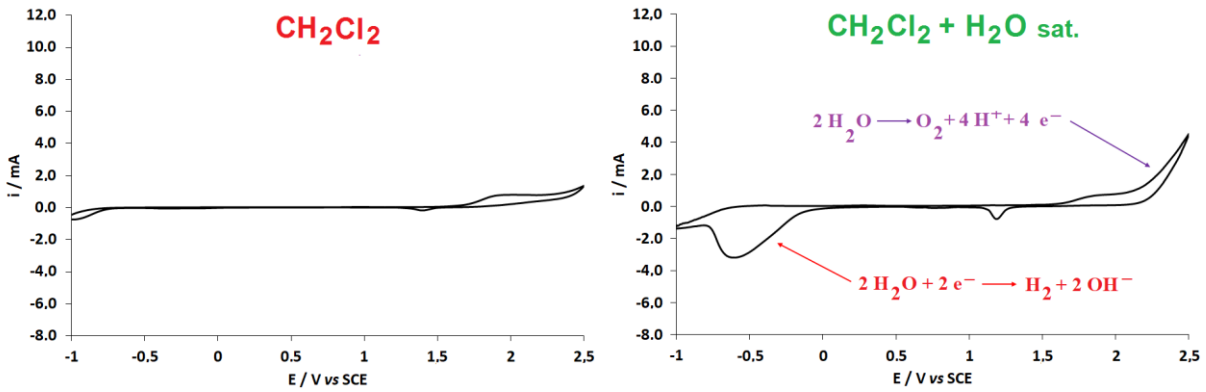

Figure 1. Cyclic voltammogram of the two solvents (CH_2Cl_2 and CH_2Cl_2 + H_2O sat.) with 0.1 M of Bu_4NClO_4. 1 scan at a scan rate of 20 mV s^{-1}.

Examples of cyclic voltammograms are available in Figure 1. In CH_2Cl_2, the cyclic voltammograms of each tested monomer are very well defined with polymer oxidation and reduction peaks typically between 0.5 V and 1.0 V *vs* SCE. In CH_2Cl_2 + H_2O sat., compared to other substituents used in the literature, the pyrene moiety allowing better resistance to the pressure induced by the gas bubbles released during the process. Indeed, pyrene participates significantly in the polymerization; it has oxidation potential close to that of thieno[3,4-*b*]thiophene, and also induces high π-stacking interactions. The cyclic voltammograms show that the more affected monomers are Thieno-C_2-Pyr and Thieno-C_8-Pyr. To better explain these last results, it was first necessary to investigate the polymer growth by SEM.

SEM images of the surfaces obtained in CH_2Cl_2 are given in Supporting Information. The surfaces are not extremely rough and the rougher surfaces are obtained with Thieno-Pyr, Thieno-C_2-Pyr and Thieno-C_{10}-Pyr. Porous structures are obtained only with Thieno-Pyr, showing its higher capacity to form porous structures even with very low water content. However, the number of porous structures is not very important but their size very large.

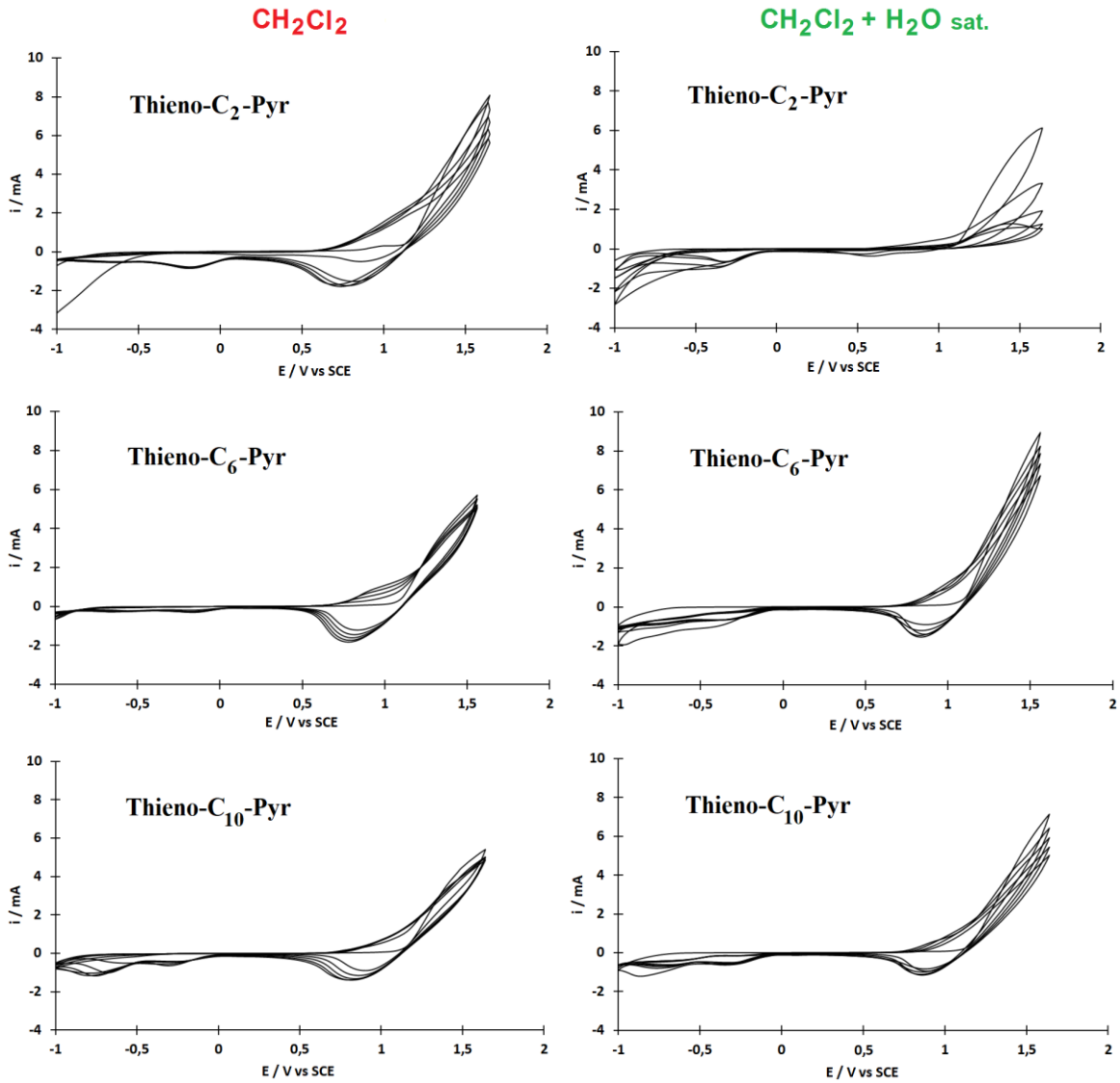

Figure 2. Example of cyclic voltammogram of monomer (Thieno-C_2-Pyr, Thieno-C_6-Pyr and Thieno-C_{10}-Pyr) in CH_2Cl_2 or CH_2Cl_2 + H_2O sat. with 0.1 M of Bu_4NClO_4. 5 scans at a scan rate of 20 mV s^{-1}.

By contrast, the surfaces obtained in CH_2Cl_2 + H_2O sat. are much rougher and porous (Figure 3 and Figure 4). A very nice change in surface structures is observed as a function of the alkyl spacer. With Thieno-Pyr, a huge number of nanotubular structures is present on the surface indicating that the polymer growth is mainly mono-dimensional (1D). The surface structures change into nanoribbons with Thieno-C_2-Pyr (2D growth), and finally hollow spheres with longer alkyl chains (3D growth). SEM images after substrate inclination allow to better visualize the change in surface morphology (Figure 4). Huge open spheres of roughly 3-4 µm in diameter are observed with intermediate alkyl spacers (Thieno-C_4-Pyr and Thieno-C_6-Pyr). The structures are much less present with Thieno-C_8-Pyr probably because the polymer

becomes too soluble in CH_2Cl_2. By contrast, very nice structures are obtained again with Thieno-C_{10}-Pyr. These last results can be explained by the presence of higher van der Waals interactions as the alkyl chain becomes sufficiently long, as already observed in literature. In order to better explain the variations in surface structures, it is important to cite previous works in the literature [45]. It was demonstrated during the polymerization of aniline in aqueous solution that it leads to the formation a trimer and this is because this molecule is asymmetrical that intermolecular attractive forces can lead to various assemblies such as nanofibers (1D growth), nanosheets (2D growth) or flower-like and urchin-like structures (3D growth), following the synthetic conditions. Here, this is the planarity of Thieno-Pyr and presence of many aromatic groups which can explain the formation of nanotubes (1D growth) because intermolecular attractive forces especially π-stacking interactions are preferential in one direction between these molecules. These interactions are reduced when an alkyl chain is placed between thieno[3,4-*b*]thiophene and pyrene leading to nanoribbons (2D growth) using Thieno-C_2-Pyr and hollow spheres (3D growth) with longer alkyl chains. These results also confirm previous works on naphthalene-substituted PheDOT showing that even the position of the substituent can affect the polymer growth [34].

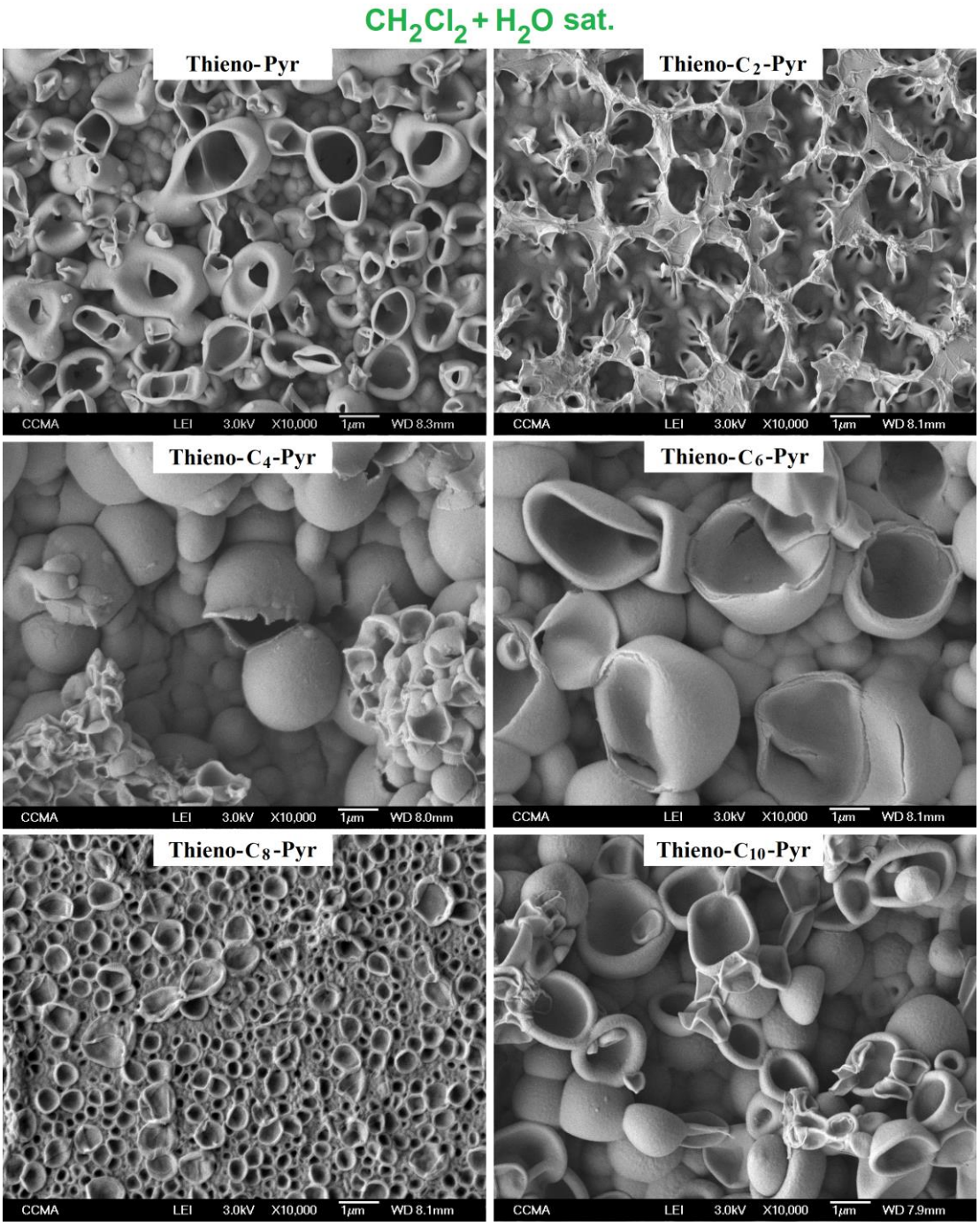

Figure 3. SEM images obtained with each investigated monomer in CH_2Cl_2 + H_2O sat. 3 scans at a scan rate of 20 mV s^{-1}.

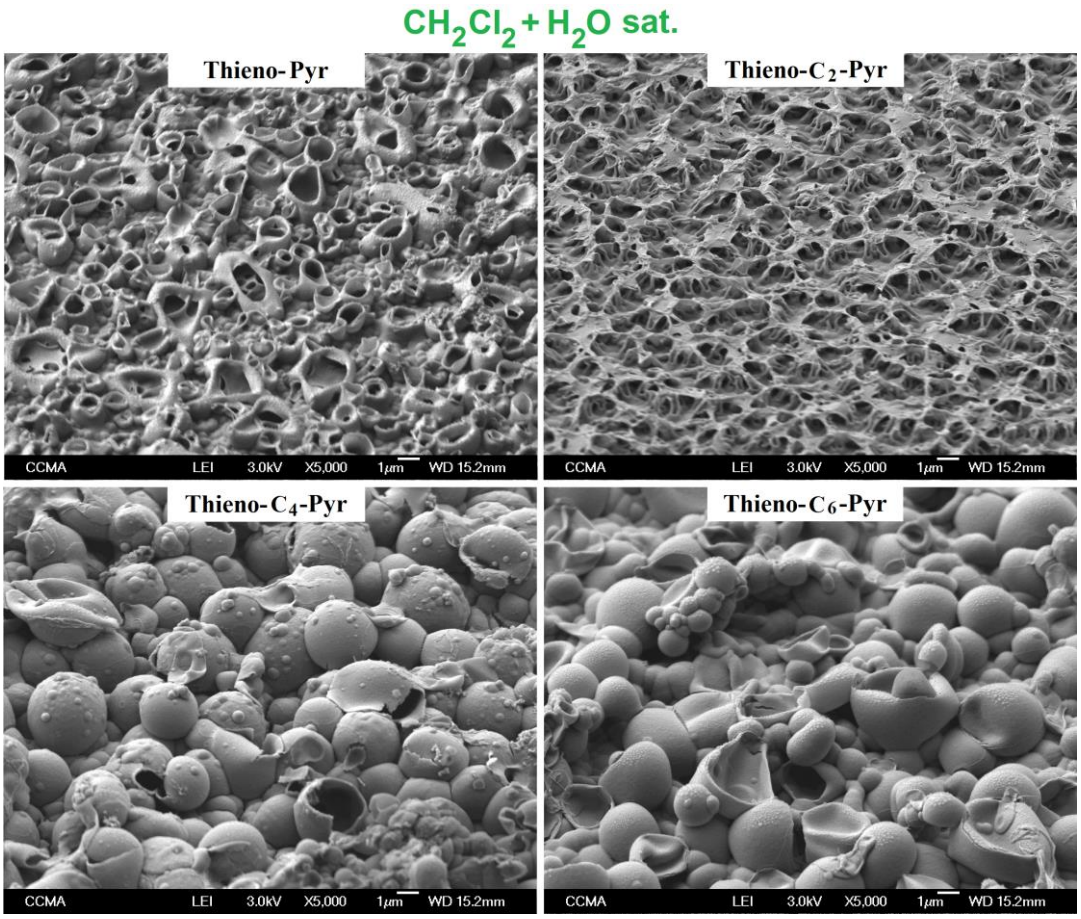

Figure 4. SEM images obtained with each investigated monomer in CH_2Cl_2 + H_2O sat. 3 scans at a scan rate of 20 mV s^{-1}. The substrates are inclined at 45°.

Moreover, with Thieno-C_6-Pyr, we have investigated the influence of H_2O content in order to better explain the formation of these huge hollow spheres. Different amount of H_2O (0 %, 35%, 65% and 100% or sat.) were studied by simply mixing CH_2Cl_2 with different amounts of CH_2Cl_2 + H_2O sat. The SEM images are given in Figure 5. It observed the presence of some nanotubular structures with 35 % H_2O while their number highly increases with 65 % H_2O leading to nanoribbons, as observed with Thieno-C_2-Pyr. In contrast, the presence of the huge open spheres are mainly observed with CH_2Cl_2 + H_2O sat.

Thieno-C_6-Pyr

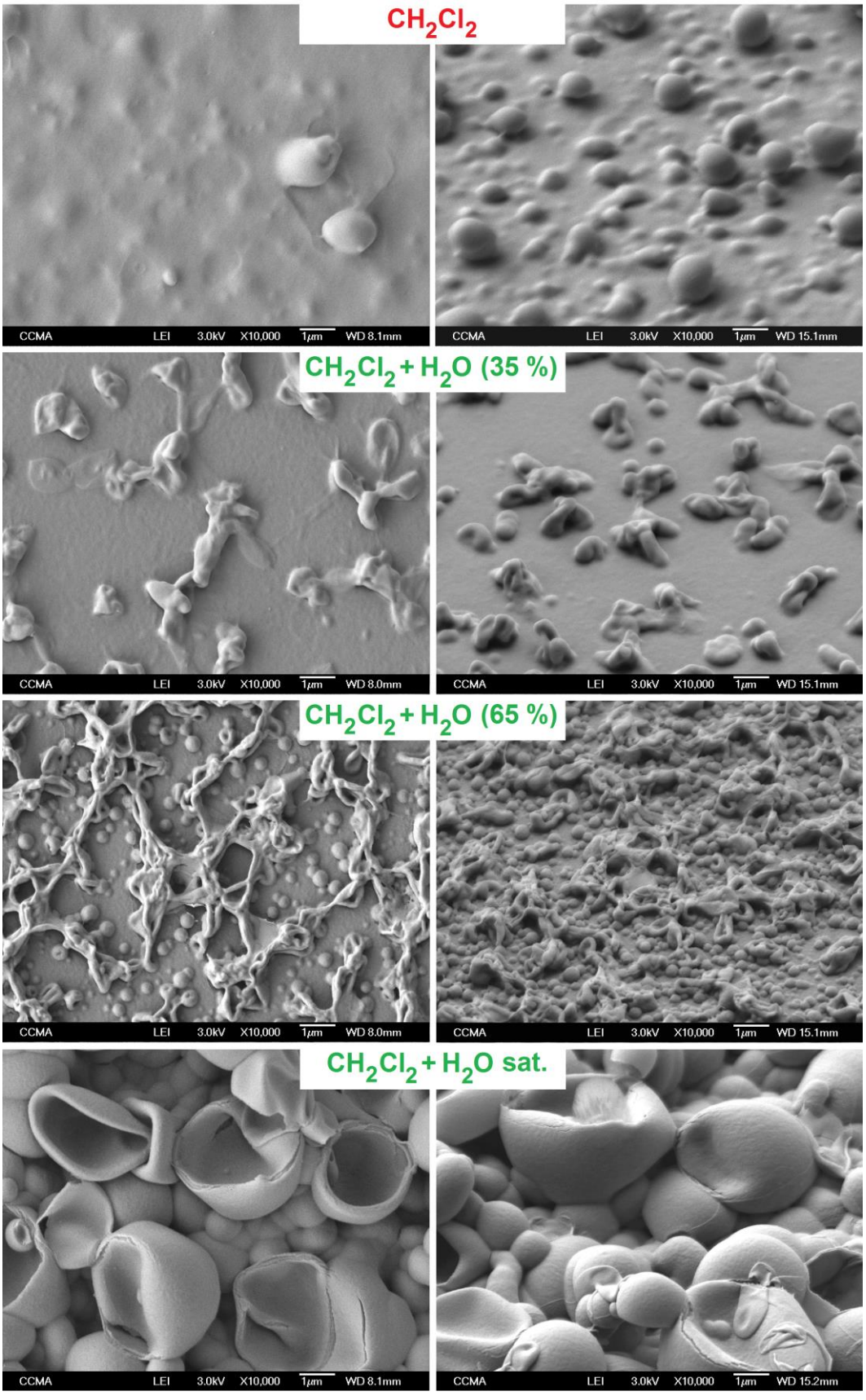

Figure 5. SEM images obtained with Thieno-C_6-Pyr as the monomer in CH_2Cl_2 and with different amount of H_2O (0 %, 35%, 65% and 100% or sat.). 3 scans at a scan rate of 20 mV s^{-1}. The substrates are not inclined (on the left) and inclined at 45° (on the right).

The wettability data are given in Table 1 and Supporting Information. The results obtained in CH_2Cl_2 show that the surfaces are not very hydrophobic, which is expected because most of these surfaces are not very rough. However, the surfaces obtained with Thieno-C_{10}-Pyr are extremely hydrophobic because of both the presence of cauliflower-like structures and long alkyl chains, which should also reduce the surface energy. The results obtained in CH_2Cl_2 + H_2O sat. show that the surfaces are not also very hydrophobic. However, the surfaces obtained with Thieno-C_2-Pyr are extremely hydrophobic (θ_w = 131.1° for 5 scans) because of the presence of ribbon-like structures, confirming previous works showing that the ribbon-like structures can lead, in certain conditions, to higher hydrophobicity that tubular-structures because an amount of air can be trapped between the ribbon-like structures [31].

Table 1. Wettability data for the polymer films obtained by cyclic voltammetry.

Polymer	Solvent	Number of deposition scans	θ_w [deg]
PolyThieno-Pyr	CH_2Cl_2	1	82.3 ± 7.8
		3	79.7 ± 8.7
		5	81.1 ± 7.1
	CH_2Cl_2 + H_2O sat.	1	96.2 ± 5.8
		3	80.2 ± 4.1
		5	104.0 ± 8.1
PolyThieno-C_2-Pyr	CH_2Cl_2	1	89.2 ±2.4
		3	98.4 ± 5.1
		5	96.0 ± 4.6
	CH_2Cl_2 + H_2O sat.	1	82.1 ± 5.0
		3	115.1 ± 1.4
		5	131.1 ± 4.0

PolyThieno-C_4-Pyr	CH_2Cl_2	1	93.3 ± 4.5
		3	93.6 ± 3.7
		5	86.1 ± 3.2
	CH_2Cl_2 + H_2O sat.	1	93.9 ± 3.0
		3	84.2 ± 4.0
		5	78.4 ± 4.1
PolyThieno-C_6-Pyr	CH_2Cl_2	1	96.5 ± 4.2
		3	102.5 ± 2.5
		5	114.2 ± 6.2
	CH_2Cl_2 + H_2O sat.	1	85.2 ± 7.1
		3	94.9 ± 8.3
		5	112.7 ± 7.3
PolyThieno-C_8-Pyr	CH_2Cl_2	1	75.5 ± 3.7
		3	88.6 ± 1.2
		5	104.1 ± 4.4
	CH_2Cl_2 + H_2O sat.	1	100.9 ± 1.4
		3	91.6 ± 2.1
		5	115.5 ± 6.4
PolyThieno-C_{10}-Pyr	CH_2Cl_2	1	89.3 ± 2.6
		3	97.3 ± 2.3
		5	132.9 ± 2.3
	CH_2Cl_2 + H_2O sat.	1	92.4 ± 2.8
		3	95.4 ± 5.7
		5	88.3 ± 3.2

Moreover, the films were also chemically characterized. Example of infrared (IR) spectra obtained with Thieno-C_6-Pyr and recorded by ATR are given in Figure 6. Peaks are present at ≈ 2800-3000 cm^{-1} for C-H stretching as well as peak at 1708 cm^{-1} for C=O. Other peaks are present at ≈ 1000-1200 cm^{-1} for example for C-O stretching.

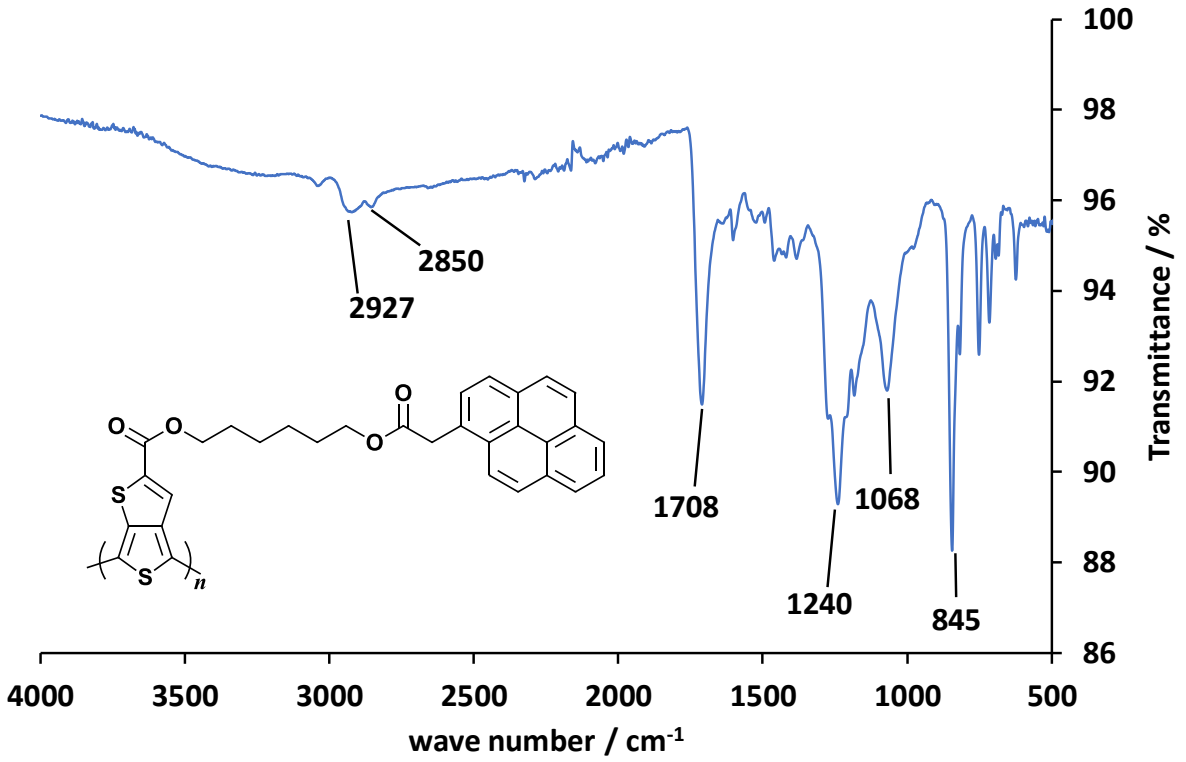

Figure 6. Infrared spectra of polymer surfaces obtained from Thieno-C_6-Pyr *via* cyclic voltammetry (5 scans) and using CH_2Cl_2 as solvent.

The films were also chemically characterized by EDX. An intense peak of the gold confirms the presence of gold on the substrate. Example of infrared (IR) spectra obtained with Thieno-C_6-Pyr and recorded by ATR are given in Figure 7. For the polymers, peaks characteristic of the presence of C, O and S are clearly present in the spectra with a much higher intensity for C peak. Moreover, very small peaks for Cl are also present, which may be due to the presence of some ClO_4^- counterions.

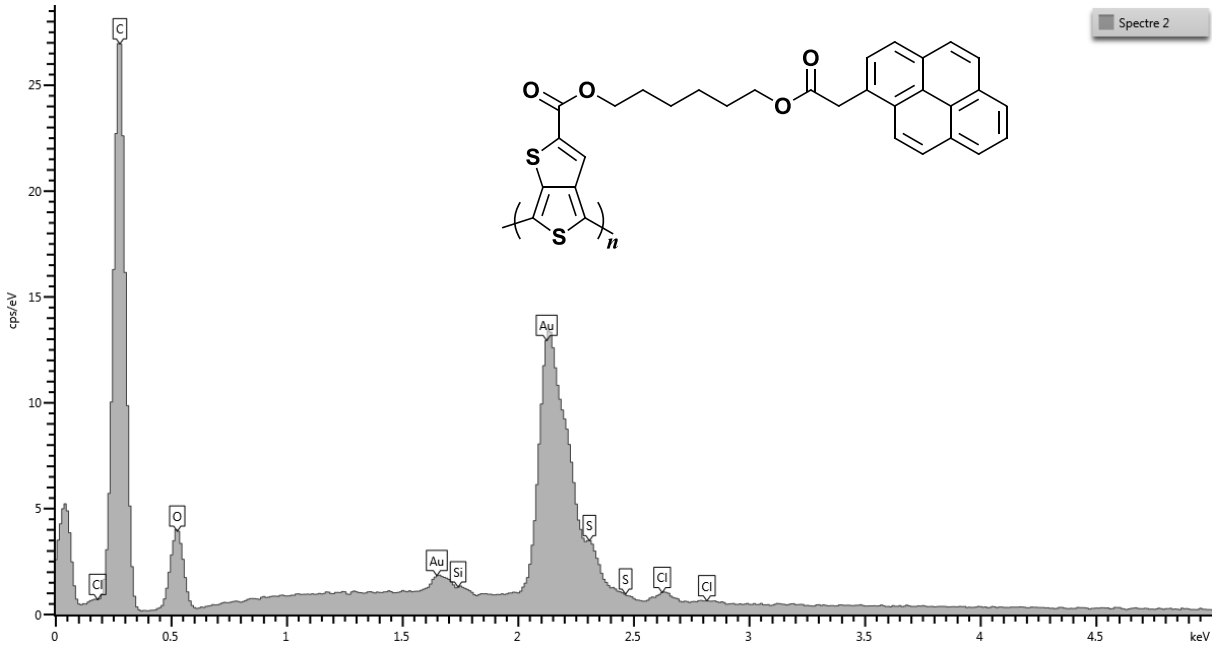

Figure 7. EDX spectra of polymer surfaces obtained from Thieno-C_6-Pyr *via* cyclic voltammetry (5 scans) and using CH_2Cl_2 as solvent.

Conclusion

Here, we explored for the first time how a simple alkyl chain can affect the polymer growth and as a consequence the resulting porous structures by templateless electropolymerization. Taking thieno[3,4-*b*]thiophene and pyrene as monomer and substituent respectively, a very nice change from nanotubular structures (1D growth) without alkyl chain to huge hollow spheres (3D growth) for longer alkyl chains ($\geq C_4H_8$) passing through ribbon-like structures (2D) for short C_2H_4 spacer, was observed. It was also necessary to add a significant amount of water for the formation of these porous structures in order to release a high amount of gas bubbles. Moreover, this change in surface structures was also observed by varying H_2O content. The higher hydrophobic properties with extremely high water adhesion were obtained with the presence of ribbon-like structures. These results could be used in various

potential applications in the future where the surface properties are dependent on the surface structures.

Acknowledgments

The group thanks Alyssia Mari from the Centre Commun de Microscopie Appliquée (CCMA, Université Nice Sophia Antipolis) for the preparation of the substrates necessary for the SEM analyses. The IR analyses were performed at the technological platform Smart City Innovation Center granted by Plan-Etat Region 2015–2020 (Provence-Alpes-Côte d'Azur).

References

[1] J. Mei, T. Liao, L. Kou, Z. Sun, Adv. Mater 29 (2017) 1700176.
[2] P. Wang, M.E. Nasir, A.V. Krasavin, W. Dickson, Y. Jiang, A.V. Zayats, Acc. Chem. Res. 52 (2019) 3018–3028.
[3] M. Xiao, W. Lai, T. Man, B. Chang, L. Li, A.R. Chandrasekaran, H. Pei, Chem. Rev. 119 (2019) 11631–11717.
[4] J.-L. Wang, J.-W. Liu, S.-H. Yu, Mater. Lett. 1 (2019) 541–548.
[5] X. Zhang, A. Wang, X. Liu, J. Luo, Acc. Chem. Res. 52 (2019) 3223–3232.
[6] J. Ren, A. Yu, P. Peng, M. Lefler, F.-F. Li, S. Licht, Acc. Chem. Res. 52 (2019) 3177–3187.
[7] A. Marmur, Langmuir 2003, 19, 8343–8348.
[8] K. Zhang, S. Huang, J. Wang, G. Liu, Angew. Chem., It. Ed. 58 (2019) 12004-12009.
[9] B. Su, Y. Tian, L. Jiang, J. Am. Chem. Soc. 138 (2016) 1727–1748.
[10] Y. Sun, Z. Guo, Nanoscale Horiz. 4 (2019) 52–76.
[11] H. Zhu, Z. Guo, W. Liu, Chem. Commun. 52 (2016) 3863–3879.
[12] Z. Cheng, J. Gao, L. Jiang, Langmuir 26 (2010) 8233–8238.
[13] K.K.S. Lau, J. Bico, K.B.K. Teo, M. Chhowalla, G.A.J. Amaratunga, W.I. Milne, G.H. McKinley, K.K. Gleason, Nano Lett. 3 (2003) 1701–1705.
[14] P. Wang, T. Zhao, R. Bian, G. Wang, H. Liu, ACS Nano 11 (2017) 12385–12391.

[15] L. Feng, Y. Zhang, J. Xi, Y. Zhu, N. Wang, F. Xia, L. Jiang, Langmuir 24 (2008) 4114–4119.
[16] K. Liu, J. Du, J. Wu, L. Jiang, Nanoscale 4 (2012) 768–772.
[17] C.R. Szczepanski, T. Darmanin, F. Guittard, Adv. Colloid Interface Sci. 241 (2017) 37–61.
[18] W. Barthlott, M. Mail, B. Bhushan, K. Koch, Nano-Micro Lett. 9 (2017) 23.
[19] L. Lee L, S.J. Park, Chem. Rev. 114 (2014) 7487–7556.
[20] H.-A. Lin, S.-C. Luo, B. Zhu, C. Chen, Y. Yamashita, H.-h. Yu, Adv. Funct. Mater. 23 (2013) 3212–3219.
[21] N. Subramanian, A. Qamar, A. Alsaadi, A.Jr. Gallo, M.G. Ridwan, J.G. Lee, S. Pillai, S. Arunachalam, D. Anjum, F. Sharipov, N. Ghaffour, H. Mishra, J. Colloid Interface Sci. 533 (2019) 723–732.
[22] A. Shumskaya, V. Bundyukova, A. Kozlovskiy, M. Zdorovets, K. Kadyrzhanov, G. Kalkabay, E. Kaniukov, J. Magn. Magn. Mater. 497 (2020) 165913.
[23] G. Kalkabay, A. Kozlovskiy, M. Zdorovets, D. Borgekov, E. Kaniukov, A. Shumskaya, J. Magn. Magn. Mater. 489 (2019) 165436.
[24] D.V. Yakimchuk, S.A. Khubezhov, V.D. Bundyukova, A.L. Kozlovskiy, M.V. Zdorovets, D.I. Shlimas, D.I. Tishkevich, E. Yu Kaniukov, Mater. Res. Express 6 (2019) 105058.
[25] C. Debiemme-Chouvy, Electrochem. Solid-State Lett. 10 (2007) E24−E26.
[26] A. Fakhry, H. Cachet, C. Debiemme-Chouvy, Electrochim. Acta 179 (2015) 297−303.
[27] C. Debiemme-Chouvy, A. Fakhry, F. Pillier, Electrochim. Acta 268 (2018) 66–72.
[28] A. Fakhry, F. Pillier, C. Debiemme-Chouvy, J. Mater. Chem. A 2 (2014) 9859−9865.
[29] L. Qu, G. Shi, J. Yuan, G. Han, F. Chen, J. Electroanal. Chem. 561 (2004) 149−156.
[30] L. Qu, G. Shi, F. Chen, J. Zhang, Macromolecules 36 (2003) 1063−1067.
[31] J. Yuan, L. Qu, D. Zhang, G. Shi, Chem. Commun. 0 (2004) 994−995.
[32] J.T. Kim, S.K. Seol, J.H. Je, Y. Hwu, G. Margaritondo, Appl. Phys. Lett. 94 (2009) 034103.
[33] B. Parakhonskiy, D. Shchukin, Langmuir 31 (2015) 9214−9218.
[34] T. Darmanin, E.L. Klimareva, I. Schewtschenko, F. Guittard, I.F. Perepichka, Macromolecules 52 (2019) 8088–8102.
[35] T. Darmanin, F. Guittard, J. Mater. Chem. A 4 (2016) 3197–3203.
[36] C.R. Szczepanski, I. M'Jid, T. Darmanin, G. Godeau, F. Guittard, J. Mater. Chem. A 4 (2016) 17308–17323.

[37] S. Bai, Q. Hu, Q. Zeng, M. Wang, L. Wang, ACS Appl. Mater. Interfaces 10 (2018) 11319–11327.
[38] O. Sane, A. Diouf, G. Morán Cruz, F. Savina, R. Méallet-Renault, S. Amigoni, S.Y. Dieng, F. Guittard, T. Darmanin, Mater. Today 31 (2019) 119–120.
[39] G. Ramos Chagas, T. Darmanin, G. Godeau, F. Guittard, Electrochim. Acta 269 (2018) 462–478.
[40] E.h.Y. Thiam, A. Dramé, S. Sow, A. Sene, C.R. Szczepanski, S.Y. Dieng, F. Guittard, T. Darmanin, ACS Omega 4 (2019) 13080–13085.
[41] S. Sow, A. Dramé, E.h.Y. Thiam, F. Orange, A. Sene, S.Y. Dieng, F. Guittard, T. Darmanin, Prog. Org. Coat. 138 (2020) 105382.
[42] G. Buemi, Bull. Chem. Soc. Jpn. 62 (1989) 1262–1268.
[43] V. S. Saji, K. K. Zong, M. Pyo, J. Photochem. Photobiol. A: Chem. 212 (2010) 81–87.
[44] Y. Wada, Y. Asada, T. Ikai, K. Maeda, T. Kuwabara, K. Takahashi, S. Kanoh, ChemistrySelect 1 (2016) 703–709.
[45] Y. Zhao, J. Stejskal, J. Wang, Nanoscale 5 (2013) 2620–2626.